Impact of PLL Control on Small-Signal Stability of Wind DFIGs Connected to Weak Grids

Régulo Ávila-Martínez, Luis Rouco, Javier García-Aguilar, Javier Renedo, Lukas Sigrist, Aurelio García-Cerrada
Instituto de Investigación Tecnológica (IIT)
ETSI ICAI, Universidad Pontificia Comillas
Madrid, Spain
{regulo.avila, luis.rouco, javier.garcia.aguilar, javier.renedo, lukas.sigrist, aurelio.garcia}@iit.comillas.edu

***Abstract* — Research into doubly-fed induction generator (DFIG) technology has yet to solve the instability that arises when DFIGs are connected to weak grids. To investigate this problem, this work used the modal analysis technique to study the impact of the phase-locked loop (PLL) control on the small-signal stability of wind-driven DFIGs and examine the sensitivity to the grid-impedance. Using a highly-detailed model, this study explains how stability can be guaranteed in terms of the ratio between the bandwidth of generator current controllers and the bandwidth of the phase-locked loop controller. Finally, the study provides practical recommendations for PLL design, based on the research findings.**

***Keywords*—Wind generators, doubly fed induction generators, phase locked loop, modal analysis, eigenvalues.**

I. INTRODUCTION

Wind generation is a mature technology representing a significant part of the generation portfolio in a number of countries, such as Denmark, Germany, Spain, United States and United Kingdom. Wind-driven Doubly Fed Induction Generators (DFIGs) (type-3 wind turbines) are currently the dominant technology for on-shore wind generation, due to the good compromise between performance and cost. Although DFIG technology is quite mature, stability problems continue to arise when DFIGs are connected to weak grids. The stability of the interaction of Phase Locked Loop (PLL) control with the rest of the system is particularly troublesome.

DFIGs are controlled using two Voltage Source Converters (VSCs) [1] (one connected to the rotor or rotor side converter, RSC, and another one connected to the grid and the stator or grid-side converter, GSC) that partially decouple the induction generator from the grid. The most extended way of controlling the GSC is the so-called vector control, where mobile d-q axes are aligned with the voltage of the grid-stator Point of Common Coupling (PCC). The GSC is synchronized to the grid using a PLL to calculate the grid angle at the PCC. One implementation of the PLL consists in making the q component of the voltage equal to zero by using a Proportional-Integral (PI) controller, which uses a synchronous reference frame (SRF) to estimate the phase angle [1]. However, more advanced PLL schemes have been proposed with the purpose of improving aspects such as the dynamic performance of the system, the performance during faults or the robustness in the presence of harmonic distortion [3], [4].

Vector control of VSCs exhibits a satisfactory performance when connected to a strong grid, but stability issues are known to arise when the VSC is connected to a weak grid. Those stability problems can be present in all applications of VSC technology: in wind turbines (either DFIG or full converter), in solar photovoltaic (PV) generators, in Flexible Alternating Current Transmission Systems (FACTS) and in VSC-based High-Voltage Direct Current systems (VSC-HVDC).

The study in [5] used small-signal stability techniques to analyse the impact of the gains of the PLL controller on the stability of a VSC-HVDC system connected to a weak grid, concluding that high gains of the PLL can produce instabilities, which is more critical for low short-circuit ratios (SCRs). The stability of a VSC-HVDC connected to a weak grid was also analysed in [6], revealing stability issues when using traditional vector control. To tackle this problem, the researchers proposed an effective control technique by using adaptive gains (gain scheduling) in the outer controllers of the VSC. Research discussed in [7] and [8] studied the dynamic behaviour of VSCs connected to weak grids using a small signal model and proposed guidelines for the selection of a proper PLL bandwidth to improve VSC system stability. The study in [9] performed small-signal analysis of a wind farm based on DFIG-type wind turbines connected to a weak grid, to study the impact of the parameters of PLL controllers. The study showed that the PLL can produce instabilities and proposes a damping controller to stabilize the system. A recent study [10] analysed the impact of PLLs on the stability of a wind farm based on full-converter-based wind turbines connected to a weak grid, showing that low SCRs can produce instabilities. The authors also proposed an indicator to assess the small-signal stability limit caused by the system strength. The study in [11] also analysed the impact of PLL control on the stability of full-converter-based wind turbines. The work identified oscillations of order 4 Hz and 30 Hz and it showed that the dominant mode depends on the PLL bandwidth. Another study [12] performed small-signal analysis of a PV generator connected to a weak grid and proposed including a compensation filter in the PLL to improve stability. The research described in [13] studied the design of the PLLs of a microgrid with VSC-based generation connected to a weak grid, concluding that slower bandwidths of the PLLs can improve stability margins.

Although these previous studies have shown that the interaction of vector control, the PLL controller and the grid is involved in the stability issues of VSCs connected to weak grids, the mechanisms that drive the system to instability (namely, the modes that are destabilized and the parameters that have more impact on stability) are still not fully understood. In response to this problem, this study investigates the small-signal stability of DFIGs using a highly detailed model that includes the detailed electromagnetic representation of the induction machine and the grid and the current controllers of the converters. Modal analysis technique is used for this purpose. Eigenvalues and participation factors are obtained and discussed in detail.

The specific contributions of this study are as follows:

- It explains how stability conditions are obtained in

terms of the ratio between the bandwidth of generator current controllers and the bandwidth of PLL control.

- It analyses the modes that can be destabilized and their participation factors.
- It analyses the effects of the sensitivity to the grid-impedance on the small signal stability.
- It offers some recommendations for PLL controller design.

This paper is an extension of preliminary results published in PES General Meeting [14].

The rest of the paper is organized as follows. Section II describes the DFIG model and the Modal Analysis Technique used in this work. Section III explains the results of the modal analysis of the DFIG model. Section IV provides the conclusions.

II. MODEL

A. DFIG-based wind turbines

Fig. 1 displays the control scheme of a wind-driven DFIG. The rotor windings are fed by a three-phase VSC with pulse width modulation that provides a three-phase voltage system of variable frequency. The variation of the frequency of rotor currents results in a variation of the rotor speed. Assuming that the stator frequency f_1 is constant, a variation of the rotor frequency f_2 results in a change of rotor speed n according to

$$s = \frac{n_1 - n}{n_1} = \frac{f_2}{f_1}$$

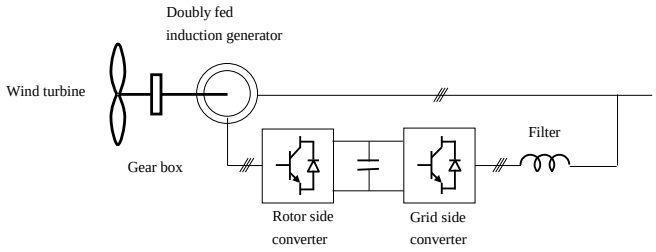

Fig. 1. Single-line diagram of a wind DFIG.

The electronic interface consists of two converters coupled through a DC link capacitor. The rotor-side converter (RSC) is used to control either the torque or the rotor speed and the rotor reactive power by means of the rotor current (see Fig. 2). The rotor current is expressed in a rotating reference frame aligned with the stator flux space vector. The component in the direct axis of the rotor current (excitation current) controls the generator reactive power. The usual strategy is to set it to zero. The component in the quadrature axis (torque current) controls the electromagnetic torque of the generator.

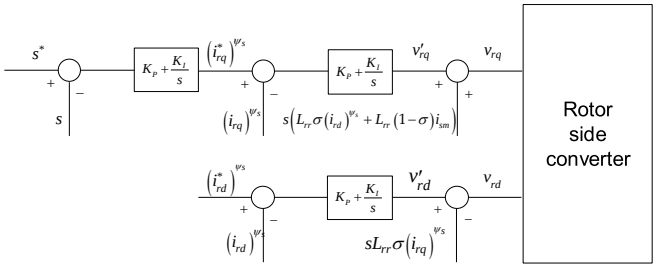

Fig. 2. Controllers of the rotor-side converter.

The stator- or grid-side converter (GSC) is used to control the overall generator reactive power and the DC capacitor voltage (see Fig. 3). The latter is controlled by the direct axis component of the GSC current while the former is controlled by quadrature axis component of this current.

A test system has been developed to investigate the interaction of Phase-Locked Loop (PLL) control with the wind-driven DFIG. The equivalent circuit of this test system is shown in Fig. 4. It includes a detailed model of the induction machine, the filter of the grid side converter, a harmonic RC filter, and the grid Thèvenin's equivalent. Equations of the grid Thèvenin's equivalent are written in a synchronous rotating reference frame whereas the DFIG equations are written in the *dq* rotating reference frame of the DFIG itself. The two reference frames are related through the PLL controller show in Fig. 5.

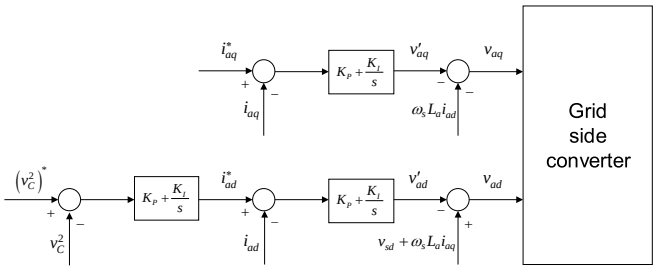

Fig. 3. Controllers of the stator-side converter

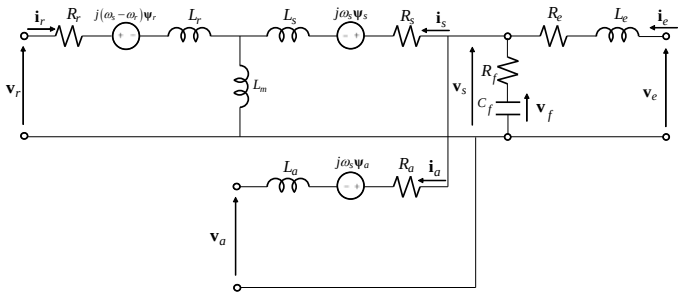

Fig. 4. Equivalent circuit of test case.

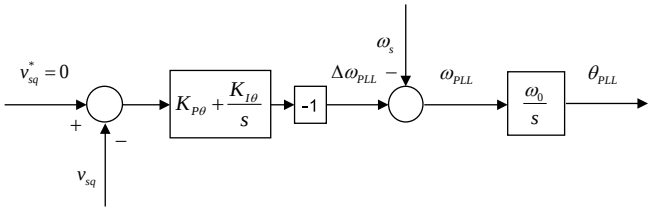

Fig. 5. PLL control loop.

The DFIG model is described by a set of non-linear differential and algebraic equations that can be written in compact form (see [15] for details) as

$$\begin{aligned} \dot{\mathbf{x}} &= \mathbf{f}(\mathbf{x}, \mathbf{z}, \mathbf{u}) \\ \mathbf{0} &= \mathbf{g}(\mathbf{x}, \mathbf{z}, \mathbf{u}) \end{aligned} \tag{1}$$

where the state variables $\mathbf{x}$, the algebraic variables $\mathbf{z}$, and the input variables $\mathbf{u}$ are (see Appendix B, for an explanation of these symbols):

$$\mathbf{x}^T = \left[\psi_{sd}\ \psi_{sq}\ \psi_{rd}\ \psi_{rq}\ \psi_{ad}\ \psi_{aq}\ s\ v_C^2\ x_{a1}\ x_{a2}\ x_{a3}\ x_{r1}\ x_{r2}\ x_s \right.$$
$$\left. v_{Cfd}\ v_{Cfq}\ \psi_{tR}\ \psi_{tI}\ x\omega_{PLL}\ \theta_{PLL} \right]$$

$$\mathbf{z}^T = \Big[i_{sd}\ i_{sq}\ i_{rd}\ i_{rq}\ i_{ad}\ i_{aq}\ v_{ad}\ v_{aq}\ i_{ad}^*\ i_{sm}\ \psi_s\ \phi$$
$$v_{sd}\ v_{sq}\ v_{sR}\ v_{sI}\ i_{fd}\ i_{fq}\ i_{ed}\ i_{eq}\ i_{eR}\ i_{eI}\ \omega_{PLL}$$
$$(v_{rd})^{\psi_s}\ (v_{rq})^{\psi_s}\ v_{rd}\ v_{rd}\ (i_{rd})^{\psi_s}\ (i_{rq})^{\psi_s}\ t_e\ p_r\ p_a\ (i_{rq}^*)^{\psi_s} \Big]$$

$$\mathbf{u} = \Big[t_m\ i_{aq}^*\ v_C^*\ (i_{rd}^*)^{\psi_s}\ s^*\ v_{eR}\ v_{eI} v_{sq}^* \Big]$$

B. Small-signal model of a DFIG

Linearizing the set of non-linear differential and algebraic equations in (1), we have:

$$\begin{bmatrix} \Delta\dot{\mathbf{x}} \\ \mathbf{0} \end{bmatrix} = \begin{bmatrix} \mathbf{A}_{11}\ \mathbf{A}_{12} \\ \mathbf{A}_{21}\ \mathbf{A}_{22} \end{bmatrix} \begin{bmatrix} \Delta\mathbf{x} \\ \Delta\mathbf{z} \end{bmatrix} + \begin{bmatrix} \mathbf{B}_1 \\ \mathbf{B}_2 \end{bmatrix} \Delta\mathbf{u}$$
$$\Delta\mathbf{y} = \begin{bmatrix} \mathbf{C}_1\ \mathbf{C}_2 \end{bmatrix} \begin{bmatrix} \Delta\mathbf{x} \\ \Delta\mathbf{z} \end{bmatrix} \tag{2}$$

The explicit linear model of the wind DFIG is obtained eliminating the algebraic variables from (2).

$$\Delta\dot{\mathbf{x}} = \mathbf{A}\Delta\mathbf{x} + \mathbf{B}\Delta\mathbf{u}$$
$$\Delta\mathbf{y} = \mathbf{C}\Delta\mathbf{x} + \mathbf{D}\Delta\mathbf{u} \tag{3}$$

As the number of state variables is 20, the state matrix is 20x20.

C. Modal Analysis

Modal analysis has been used to assess the small-signal stability of the DFIG. Modal analysis calculates not only the eigenvalues but also the right and left eigenvectors of the state matrix $\mathbf{A}$. From the right and left eigenvectors, participation factors can easily be calculated to find the relationships between eigenvalues and state variables.

The right and left eigenvectors ($\mathbf{v}_i$ and $\mathbf{w}_i$ respectively) corresponding to the eigenvalue λ_i of the state matrix $\mathbf{A}$ are defined according to

$$\mathbf{A}\mathbf{v}_i = \mathbf{v}_i \lambda_i$$
$$\mathbf{w}_i^T \mathbf{A} = \lambda_i \mathbf{w}_i^T \tag{4}$$

The participation factor of the j-th variable in the i-th mode is defined as [16]

$$p_{ji} = w_{ji} v_{ji} \tag{5}$$

The participation factor p_{ji} is a dimensionless measure of the participation of the j-th variable in mode i-th and it is useful to assess the impact of control parameters on the eigenvalues of the system.

III. Results

The test system consists of a 100 MVA DFIG connected to an infinite grid, as shown in Fig. 6. The DFIG is connected to the point of common coupling (bus 2) through a 220/0.69 kV transformer. The initial operating point of the DFIG is presented in TABLE I and system data are provided in TABLE VI in Appendix A.

TABLE I. Initial values of operation point

P_1 (MW)	Q_1 (MVAR)	V_1 (pu)	*s (%)*
100.00	0.00	1.0137	-4.25%

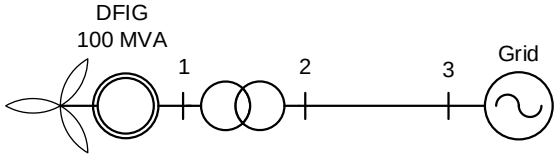

Fig. 6. DFIG connected to an infinite grid.

The short-circuit ratio (SCR) at the connection point of the DFIG (at bus 1, before the transformer) will be used to assess the strength of the grid. The SCR is defined as [17]:

$$SCR = \frac{1}{z_{th}} \tag{6}$$

where z_{th} is the magnitude of the equivalent impedance of the grid, written in pu with respect to the nominal bases of the DFIG. Since the SCR is calculated at bus 1, the equivalent impedance includes the impedance of the transformer and that of the line ($\overline{z}_{th} = \overline{z}_{t,12} + \overline{z}_{l,23}$). When the SCR is changed, the criterion used in this work is to maintain the relative value between the inductive and resistive parts of the impedance (X/R) constant. In this case study, X/R=10.

This study analyses the effect of grid impedance variation on small signal system stability. The grid impedance corresponds to the impedance of line 2-3 of Fig. 6. Two cases will be considered:

- The impact of the PLL bandwidth (ω_{nPLL}) on small-signal stability, while the current controller bandwidth (ω_{nc}) and SCR values remain fixed.
- The impact of SCR values on small-signal stability, while the bandwidth of the current and PLL controllers remain fixed.

A. Impact of the PLL bandwidth:

Two scenarios are considered:

- DFIG connected to a strong grid: SCR=10
- DFIG connected to a weak grid: SCR=2

The bandwidth values employed in this study broadly correspond to current practice in industry [18]. The current controller bandwidth is set at 2000 rad/s and the bandwidth of the outer controllers are set at a tenth of this value. The PLL bandwidth tested was changed from 10-100% of the current controller bandwidth (i.e. from 200-2000 rad/s).

In the case of a DFIG connected to a strong grid (low grid impedance), a SCR at the PCC of 10 is assumed (grid impedance of 0.1 pu). The bandwidth of the PLL controller was set at 1200 rad/s (60% of ω_{nc}). This case will be referred to as the base case of Fig. 7, marked with a red square.

TABLE II presents the modes of the system of the base case, while TABLE III presents the participation factors. All

modes are stable. Modes 1 and 8 are the ones with the lowest damping ratio. Mode 1 relates to the interaction of the stator flux, the grid current and voltage at the PCC as shown by the participation factors in TABLE III. The PLL state variables have significant participation factors in the mode 7. Mode 8 belongs to stator variables and has the lowest damping ratio, but it is always stable for all values of the bandwidth of the PLL controller.

TABLE II. LOW GRID IMPEDANCE CASE. MODES.

Number	Real	Imaginary	Damping (%)	Frequency (Hz)
1	-284.80	4138.28	6.87	660.19
2	-528.94	3492.78	14.97	562.23
3	-1010.48	1898.10	46.99	342.23
4	-970.61	1468.35	55.14	280.14
5	-1400.00	1428.29	70.00	318.31
6	-1170.70	1302.66	66.84	278.75
7	-868.36	863.63	70.90	194.92
8	-0.20	311.93	0.06	49.64
9	-141.31	143.22	70.23	32.02
10	-133.93	132.66	71.05	30.00

TABLE III. LOW GRID IMPEDANCE CASE. PARTICIPATION FACTORS.

Variables	Mode									
	1	2	3	4	5	6	7	8	9	10
Psi_sd	0.5544	0.5843	0.6286	0.6416	0	0.3006	0.4898	0.4881	0.0043	0.0042
Psi_sq	0.0770	0.0747	0.0466	0.1988	0	0.0353	0.0062	0.4948	0.0018	0.0009
Psi_rd	0.4562	0.6130	0.1575	0.3540	0	0.5024	0.0264	0.0045	0.0031	0.0087
Psi_rq	0.1259	0.1493	0.0804	0.4436	0	0.0977	0.2157	0.0006	0	0
Psi_ad	0.0162	0.0176	0.5089	0.1526	0	0.3786	0.0014	0	0.0030	0.0095
Psi_aq	0	0	0	0	0.7001	0	0	0	0	0
s	0.0037	0.0083	0.0710	0.0080	0	0.0585	0.0013	0.0050	0.5741	0.1274
v_c2	0.0157	0.0159	0.2287	0.0635	0	0.0900	0.0017	0.0047	0.1525	0.5034
x_a1	0	0	0	0	0.7001	0	0	0	0	0
x_a2	0.0055	0.0071	0.3813	0.1444	0	0.4131	0.0019	0.0001	0.0017	0.0048
x_a3	0.0005	0.0006	0.0157	0.0054	0	0.0077	0.0002	0.0020	0.1521	0.5409
x_r1	0.0164	0.0327	0.0856	0.7589	0	0.1595	0.0460	0.0006	0.0001	0.0002
x_r2	0.0141	0.0428	0.4075	0.0520	0	0.3857	0.0075	0.0005	0.0023	0.0070
x_s	0.0001	0.0003	0.0049	0.0007	0	0.0050	0.0002	0.0021	0.5725	0.1369
v_cd	0.2489	0.3150	0.0604	0.0067	0	0.0135	0.0010	0	0	0.0001
v_cq	0.2942	0.2738	0.0407	0.1542	0	0.0146	0.0963	0	0	0
Psi_tr	0.2097	0.2363	0.1501	0.0078	0	0.0544	0.0086	0.0188	0.0699	0.0940
Psi_ti	0.2150	0.2181	0.0573	0.2750	0	0.0203	0.0390	0.0476	0.0092	0.0074
x_bw_pll	0.0041	0.0125	0.0366	0.0563	0	0.0324	0.7083	0	0	0.0003
x_th_pll	0.1480	0.1855	0.1161	0.6432	0	0.0556	0.9553	0.0388	0.0729	0.0622

Fig. 7 shows the evolution of the modes when the PLL bandwidth is changed from 200 rad/s to 2000 rad/s. The base case corresponds to a 1200-rad/s PLL bandwidth (60% of the current controller bandwidth) and it is marked with a red square. The system is always stable, even if the PLL bandwidth is high. Mode 1 in TABLE II tends to move to the right-hand side of the complex plane as the PLL bandwidth increases. This mode is related to the interaction of the stator flux, the rotor flux, the grid current, voltage at the PCC and the state variables of the PLL, as shown by the participation factors of TABLE III. The rest of the modes are not problematic.

In the case of a DFIG connected to a weak grid (high grid reactance), a SCR of 2 is assumed (equivalent impedance of 0.5 pu). The PLL bandwidth was made equal to 600 rad/s. This case will be referred to as the base case of the Fig. 8 and it is marked with a red square.

TABLE IV presents the base case modes, while TABLE V presents the participation factors. All modes are stable. Mode 8 has the lowest damping ratio. This mode is related to the interaction of the stator flux, the grid current and the PLL state variables, as shown by the participation factors in TABLE V. The state variables of the PLL have significant participation factors in modes 6 and 7 and also have a relevant participation in modes 1 and 3.

Fig. 8 shows the evolution of the modes when the PLL bandwidth changed from 200 rad/s to 2000 rad/s. The base case corresponds to a 600-rad/s PLL bandwidth (30% of the current controller bandwidth) and it is marked with a red square. The system becomes unstable if the PLL bandwidth is too fast in comparison with the bandwidth of the inner current controller. For example, unlike in the case of SCR=10, for a SCR of 2 the system becomes unstable if the PLL bandwidth is 1200 rad/s (60% of the bandwidth of the inner current controller). Mode 6 in TABLE IV moves to the right-hand side of the complex plane as the bandwidth of the PLL controller increases, producing the instability. This mode is related to the interaction of the stator flux, rotor flux, the grid current, voltage at the PCC and the PLL state variables, as shown by the participation factors in TABLE V.

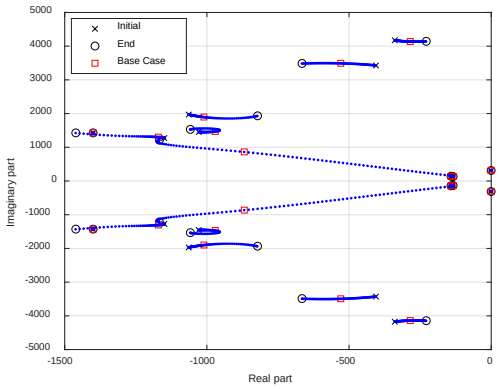

Fig. 7. Low grid impedance. Evolution of the modes as the bandwidth of PLL control is changed from 200 rad/s to 2000 rad/s. The bandwidth of PLL control in the base case is 1200 rad/s (marked with a red square).

TABLE IV. HIGH GRID IMPEDANCE. MODES.

Number	Real	Imaginary	Damping (%)	Frequency (Hz)
1	-1369.34	2541.02	47.44	459.40
2	-1077.61	2539.37	39.06	439.04
3	-460.34	1903.82	23.50	311.74
4	-1400.00	1428.29	70.00	318.31
5	-1002.79	1203.30	64.02	249.30
6	-75.44	861.53	8.72	137.64
7	-447.56	459.28	69.79	102.06
8	-2.79	304.28	0.92	48.43
9	-150.05	143.61	72.25	33.06
10	-92.50	104.23	66.38	22.18

TABLE V. HIGH GRID IMPEDANCE. PARTICIPATION FACTORS.

Variables	Mode									
	1	2	3	4	5	6	7	8	9	10
Psi_sd	1.1082	1.6921	0.6137	0	0.2058	0.6114	0.5085	0.4647	0.0177	0.0432
Psi_sq	0.0902	0.4998	0.1999	0	0.0359	0.1932	0.0153	0.5053	0.0108	0.0300
Psi_rd	1.1777	1.6655	0.3868	0	0.3494	0.2872	0.1203	0.0231	0.0380	0.0530
Psi_rq	0.0880	0.7425	0.1990	0	0.0447	0.0939	0.0711	0.0027	0.0006	0.0014
Psi_ad	0.1992	0.1962	0.4006	0	0.4474	0.0155	0.0009	0.0002	0.0060	0.0044
Psi_aq	0	0	0	0.7001	0	0	0	0	0	0
s	0.0522	0.0310	0.0711	0	0.0683	0.0244	0.0044	0.0171	0.4621	0.2095
v_c2	0.1068	0.1202	0.3886	0	0.2262	0.0870	0.0064	0.0247	0.2898	0.2475
x_a1	0	0	0	0.7001	0	0	0	0	0	0
x_a2	0.1139	0.1114	0.2746	0	0.5084	0.0152	0.0012	0.0006	0.0035	0.0012
x_a3	0.0054	0.0063	0.0288	0	0.0219	0.0144	0.0017	0.0105	0.2879	0.3054
x_r1	0.0452	0.3652	0.1404	0	0.0643	0.1898	0.0515	0.0029	0.0010	0.0026
x_r2	0.2837	0.0735	0.2857	0	0.4077	0.0595	0.0116	0.0017	0.0023	0.0060
x_s	0.0026	0.0016	0.0053	0	0.0066	0.0040	0.0011	0.0073	0.4591	0.2587
v_cd	0.2743	0.0735	0.3073	0	0.0522	0.1010	0.0067	0.0007	0.0002	0.0047
v_cq	0.0615	0.5960	0.1993	0	0.0128	0.1807	0.1228	0.0002	0.0003	0.0005
Psi_tr	0.0485	0.1557	0.2878	0	0.0623	0.0147	0.0136	0.1573	0.0213	0.1418
Psi_ti	0.0548	0.1318	0.0537	0	0.0044	0.6373	0.1740	0.2045	0.0362	0.0289
x_bw_pll	0.0154	0.0225	0.0266	0	0.0100	0.0936	0.7029	0.0005	0.0024	0.0038
x_th_pll	0.0264	0.2564	0.1946	0	0.0130	1.1468	1.2120	0.1942	0.0589	0.0395

The analysis concludes that, when the impedance of the grid is low, a bandwidth of 60% or lower (i.e. 10-60%) is normally required to allow the PLL controller to maintain an acceptable stability margin. However, when the impedance of the grid is high, a bandwidth of 30% or lower (i.e. 10-30%) is normally required, especially if the current controller bandwidth is high (2000 rad/s).

B. Impact of the value of the SCR:

Two cases have been considered in this section:

- A 1200-rad/s PLL bandwidth (60% of the current controller bandwidth)
- A 600 rad/s bandwidth(30% of the current controller bandwidth)

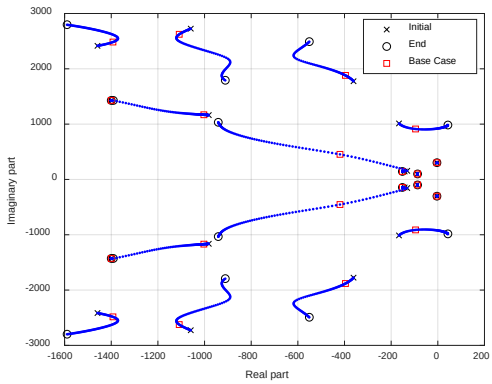

Fig. 8. High grid impedance. Evolution of the modes as the bandwidth of PLL control is changed from 200 rad/s to 2000 rad/s. The bandwidth of PLL control in the base case is 600 rad/s (marked with a red square).

Fig. 9 shows how system modes change when the SCR decreased from 10 to 2. The figure shows the same system when two cases of PLL bandwidth are considered. In the first case (in blue) with a 1200 rad/s PLL bandwidth (60% of the current controller bandwidth), the system is stable up to certain values of SCR. In the second case (in red) with a 600 rad/s PLL bandwidth (30% of the current controller bandwidth), the system is always stable, even if the SCR at the PCC is very low. Modes 4 and 6, in TABLE II and TABLE IV respectively, move to the right-hand side of the complex plane as the SCR decreases. These modes are related to the interaction of the stator flux, rotor flux, the grid current, voltage at the PCC and the PLL state variables as shown by the participation factors of TABLE III and TABLE V. The rest of the modes are not problematic.

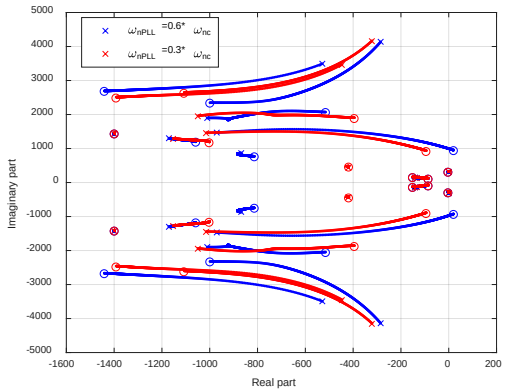

Fig. 9. Evolution of the modes as the SCR connection is changing from 10 to 2. The current controller bandwidth is 2000 rad/s. The bandwidth of the PLL control is 1200 rad/s (blue) and 600 rad/s (red).

Finally, Fig. 10 shows the time response of the q component of the GSC current (i_{aq}) of a DFIG connected to a weak grid (SCR = 2), using a non-linear model. A step of 0.01 pu is applied to the set point of i_{aq} at t=1s. Fig. 10 shows the response of the system when two cases of PLL bandwidth are considered. In the first case (in blue) with a 1200 rad/s PLL bandwidth, the system is unstable. In the second case (in red) with a 600 rad/s PLL bandwidth, the system is stable. Results confirm the conclusions obtained by modal analysis.

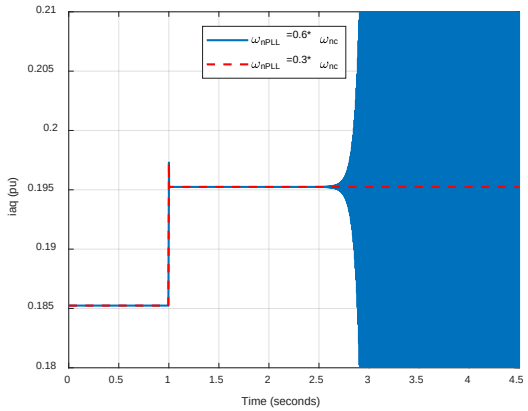

Fig. 10. Time simulation of the q component of the GSC current (i_{aq}) of a DFIG connecte to a weak grid (SCR = 2) when a step of 0.01 pu is applied at 1 second. The current controller bandwidth is 2000 rad/s. The bandwidth of the PLL control is 1200 rad/s (blue) and 600 rad/s (red).

Two conclusions can be drawn from this analysis: on the one hand, if the PLL bandwidth is 60% of the current controller bandwidth, the system becomes unstable when it is connected to a weak grid; on the other hand, the system is always stable when a lower PLL bandwidth is considered (30% of the current controller bandwidth).

IV. Conclusion

This study uses the Modal Analysis Technique to investigate the impact of the PLL on small-signal stability in a highly detailed wind-driven DFIG model. There are two main findings. Firstly, if the DFIG is connected to a strong grid (low grid impedance) and the current controller bandwidth is high (e.g. 2000 rad/s), the system is stable if the PLL bandwidth is smaller than the current controller bandwidth (e.g. 60%). This means that the PLL bandwidth can be 60% and even greater than the current controller bandwidth. Secondly, if the DFIG is connected to a weak grid (high grid impedance) and the current controller bandwidth is high, the PLL bandwidth must be less than 30% of the current controller bandwidth in order to maintain system stability. Hence, a reasonable design of the PLL bandwidth would be 10-30% of the current controller bandwidth.

In summary, the stability of a DFIG connected to a grid using a PLL in the GSC will depend on the strength of the grid and on the design of the bandwidth of both current and PLL controllers.

Acknowledgments

This work has been funded by the Instituto de Investigación Tecnológica (IIT), ETSI ICAI, Universidad Pontificia Comillas and by the Spanish Government through projects RTC-2017-6074-3 and RTI2018-098865-B-C31.

References

[1] A. Yazdani, and R. Iravani, *Voltage-Sourced Converters in Power Systems: Modeling, Control, and Applications*, IEEE Press/John Wiley, 2010.

[2] R. Teodorescu, M. Liserre, and P. Rodríguez, *Grid Converters for Photovoltaic and Wind Power Systems*, IEEE Press/John Wiley, 2007.

[3] H. A. Pereira, A. F. Cupertino, C. A. D. S. G. Ribeiro, and S. R. Silva, "Influence of PLL in wind parks harmonic emissions," *Proc. IEEE/PES Conference on Innovative Smart Grid Technology (ISGT), Sao Paulo, Brazil*, pp. 1-8.

[4] D. Jovcic, "Phase Locked Loop System for FACTS," *IEEE Transactions Power Systems*, vol. 13, no. 3, pp. 1116–1124, 2003.

[5] J. Z. Zhou, H. Ding, S. Fan, Y. Zhang, and A. M. Gole, "Impact of short-circuit ratio and phase-locked-loop parameters on the small-signal behavior of a VSC-HVDC converter," *IEEE Transactions Power Delivery*, vol. 29, no. 5, pp. 2287–2296, 2014.

[6] A. Egea-Alvarez, S. Fekriasl, F. Hassan and O. Gomis-Belmunt, "Advanced Vector Control for Voltge Source Converters Connected to Weak Grids," *IEEE Transactions Power Systems*, vol. 30, no. 6, pp. 3072–3081, 2015.

[7] G. Wu, H. Sun, X. Zhan, A. Egea-Alvarez, B. Zhao, S. Xu, S. Wang and X. Zhou, "Parameter Design Oriented Analysis of the Current Control Stability of the Weak-Grid-Tied VSC," *IEEE Transactions on Power Delivery*, doi: 10.1109/TPWRD.2020.3009517.

[8] J. F. Morris, K. H. Ahmed and A. Egea-Alvarez, "Analysis of Controller Bandwidth Interactions for Vector-Controlled VSC Connected to Very Weak AC Grids," *IEEE Journal of Emerging and Selected Topics in Power Electronics*, available online: doi: 10.1109/JESTPE.2020. 3031203, pp. 1-12, 2020.

[9] J. Liu, W. Yao, J. Wen, J. Fang, L. Jiang, H. He, and S. Cheng, "Impact of Power Grid Strength and PLL Parameters on Stability of Grid-Connected DFIG Wind Farm," *IEEE Transactions on Sustainable Energy*, available online: doi: 10.1109/TSTE.2019.2897596, pp. 1-12, 2019.

[10] W. Du, W. Dong, and H. F. Wang, "Small-signal Stability Limit of a Grid-connected PMSG wind Farm Dominated by the Dynamics of PLLs," *IEEE Transactions on Power Systems*, available online: doi: 10.1109/TPWRS.2019.2946647, pp. 1-12, 2019.

[11] L. Fan and Z. Miao, "Wind in Weak Grids: 4 Hz or 30 Hz Oscillations?," *IEEE Transactions on Power Systems*, vol. 33, no. 5, pp. 5803-5804, Sept. 2018, doi: 10.1109/TPWRS.2018.2852947.

[12] M. Berg, A. Aapro, R. Luhtala, and T. Messo, "Small-Signal Analysis of Photovoltaic Inverter with Impedance-Compensated Phase-Locked Loop in Weak Grid," *IEEE Transactions on Energy Conversion*, available online: doi: 10.1109/TEC.2019.2944947, pp. 1-10, 2019.

[13] K. Nakul Narayanan, S. Shan, and L. Umanand, "Stability Analysis of Phase Locked Loop Controllers for Grid Tied Inverters in Weak Microgrids," *Proc. IEEE/PES International Conference on Power Electronics, Drives and Energy Systems (PEDES)*, Chennai, India, 2019, pp. 1-5.

[14] R. Ávila-Martínez, L. Rouco, J. García Aguilar, J. Renedo, L. Sigrist, "Impact of PLL control on small-signal stability of wind DFIGs," Proc. IEEE/PES General Meeting *(PESGM)*, Montreal, Canada, 3-6 August 2020, pp. 1-5

[15] L. Rouco, and J. L. Zamora, "Dynamic patterns and model order reduction in small-signal models of doubly fed induction generators for wind power applications," in *IEEE/PES General Meeting* , Montreal, Quebec, Canada, 2006, pp. 1-6.

[16] I.J. Pérez-Arriaga, G.C. Verghese, and F.C. Schweppe, "Selective Modal Analysis with Applications to Electric Power Systems. Part I: Heuristic Introduction. Part II: The Dynamic Stability Problem". *IEEE Transactions on Power Apparatus and Systems*, Vol. PAS-101, No. 9, September 1982, pp. 3117-3134.

[17] L. Zhang, L. Harnefors and H-S. Nee, "Interconnection of Two Very Weak AC Systems by VSC-HVDC Links Using Power-Synchronization Control," *IEEE Transactions on Power Systems*, vol. 26, no. 1, pp. 344-355, 2011.

[18] L. Fan, R. Kavasseri, Z. L. Miao and C. Zhu, "Modeling of DFIG-Based Wind Farms for SSR Analysis," *IEEE Transactions on Power Delivery*, vol. 25, no. 4, pp. 2073-2082, 2010.

APPENDIX A:

$\mathbf{v}_s = v_{sd} + jv_{sq}$: stator voltage.

$\mathbf{v}_r = v_{rd} + jv_{rq}$: rotor voltage.

$\mathbf{v}_a = v_{ad} + jv_{aq}$: stator converter voltage.

$\mathbf{i}_s = i_{sd} + ji_{sq}$: stator current.

$\mathbf{i}_r = i_{rd} + ji_{rq}$: rotor current.

$\mathbf{i}_a = i_{ad} + ji_{aq}$: stator converter current.

$\boldsymbol{\psi}_s = \psi_{sd} + j\psi_{sq}$: stator flux.

$\boldsymbol{\psi}_r = \psi_{rd} + j\psi_{rq}$: rotor flux.

$\boldsymbol{\psi}_a = \psi_{ad} + j\psi_{aq}$: stator converter flux.

R_s , R_r : stator and rotor resistances.

L_s , L_r : stator and rotor leakage inductance.

L_m : magnetizing reactance.

R_a , L_a : resistance and inductance of stator converter connecting filter.

R_t , L_t : resistance and inductance of the connection transformer.

ω_0 : speed base $\omega_0 = 2\pi f_0$.

ω_s : synchronous speed $\omega_s = 1$.

s : slip.

t_m : mechanical torque.

t_e : electromagnetic torque.

R_e , L_e : resistance and inductance of grid Thèvenin equivalent.

R_f , C_f : resistance and capacitance of filter.

$\mathbf{i}_e = i_{eR} + ji_{eI}$: grid current.

$\boldsymbol{\psi}_e = \psi_{eR} + j\psi_{eI}$: grid flux.

$\mathbf{v}_e = v_{eR} + jv_{eI}$: Thèvenin voltage.

$\mathbf{i}_f = i_{fd} + ji_{fq}$: filter currrent.

$\mathbf{v}_{Cf} = v_{Cfd} + jv_{Cfq}$: filter capacitor voltage.

ω_{PLL} : PLL speed.

θ_{PLL} : PLL angle.

APPENDIX B:

Data of the system are provided in TABLE VI.

TABLE VI. SYSTEM DATA

Parameters	(pu)
R_s	0.01
L_s	0.15
R_r	0.01
L_r	0.15
L_m	0.5
R_a	0.06
L_a	0.6
R_f	0.01
C_f	0.085
R_t	0.001
L_t	0.15